

Full paper

Anisotropic nanogenerator for anticounterfeiting and information encrypted transmission

Xiao-Xiong Wang^{a,1}, Ning Wang^{a,1}, Huijing Qiu^a, Weizhi Song^a, Qi Liu^a, Zhiyong Fan^b, Miao Yu^{a,c}, Seeram Ramakrishna^d, Yun-Ze Long^{a,e,*}

^a Collaborative Innovation Center for Nanomaterials & Devices, College of Physics, Qingdao University, Qingdao, 266071, China

^b Department of Electronic & Computer Engineering, The Hong Kong University of Science & Technology, Kowloon, Hong Kong, China

^c Department of Mechanical Engineering, Columbia University, New York, NY, 10027, USA

^d Center for Nanofibers & Nanotechnology, National University of Singapore, Singapore

^e Collaborative Innovation Center for Eco-Textiles of Shandong Province, Qingdao University, Qingdao, 266071, China



ARTICLE INFO

Keywords:

Triboelectric nanogenerator
Anisotropy
Anticounterfeiting
Encryption
Electrospinning
Fiber membrane

ABSTRACT

Nanogenerators can provide power for independent small systems, so they have great flexibility. Among them, triboelectric nanogenerator (TENG) has gained wide attention due to its high output energy density. However, traditional TENGs don't show variation of output signal when the relative direction of the friction layers changes. Through electrospinning aligned polymer nanofibers, we obtained anisotropic TENG (A-TENG), which has better mechanical strength than the disordered electrospun TENG. This anisotropic TENG can be used as self-powered angle sensor. The appearance of A-TENG is the same along different directions, which makes it applicable for anticounterfeiting by measuring the relative output along different directions by using another piece of ordered nanofibers. Meanwhile, A-TENG can also be used for information encryption. This work provides an idea that new nanogenerators can be designed based on some common physical effects.

1. Introduction

With the development of modern technology, electronic systems with smaller volumes, better coupling with the skin, better safety and biocompatibility have received wide attention [1]. As an ideal energy power for such systems, nanogenerators have received extensive attention by collecting excess mechanical energy from the environment to power these electronic systems [2,3]. Common nanogenerators include triboelectric nanogenerators (TENG) [4–11], piezoelectric nanogenerators [12–19], pyroelectric nanogenerators [20–25], and electrostatic induction nanogenerators [26,27]. Among these nanogenerators, TENG is the most excellent nanogenerator due to its high output power and output voltage [28,29], and the open circuit voltage can often reach thousands of volts [30].

Electrospinning technology is a convenient and scalable technology for the preparation of nanofibers and is therefore used to prepare TENG for a variety of different applications [31,32]. The rough surface and gas permeability of the fiber membrane can enhance the output effect and wearability of the TENG [33,34]. As a nanofiber molding technology,

electrospinning technology can fully control the morphology and arrangement of fibers. For example, near-field electrospinning technology can be used to prepare single fiber [35,36], while parallel electrodes or high-speed rollers can be used to collect ordered nanofibers. From a physical theory, the orderly arrangement will greatly improve the mechanical properties of the fibers [37]. For TENG, the change in the relative angle of the fibers will cause a change in the effective contact area, resulting in different output effects.

Banknotes, products and documents counterfeited by counterfeiting methods not only violate the interests of the original creators, but also circumvent supervision. Therefore, they are extremely harmful, and effective anticounterfeiting measures are urgently needed. At its core, anticounterfeiting technology is difficult to replicate and easy to authenticate. In this work, we used the high-speed roller to prepare the TENG of orderly arranged nanofibers, which greatly improved the mechanical strength and tensile properties of this TENG. This TENG has the characteristics of anisotropic output. By adjusting the relative direction of the electrospun nanofibers, the output behavior can be changed. Considering that the membrane appearance along the two directions is

* Corresponding author. Collaborative Innovation Center for Nanomaterials & Devices, College of Physics, Qingdao University, Qingdao, 266071, China.

E-mail addresses: yunze.long@qdu.edu.cn, yunze.long@163.com (Y.-Z. Long).

¹ These two authors contributed equally to this work.

<https://doi.org/10.1016/j.nanoen.2020.104572>

Received 11 December 2019; Received in revised form 21 January 2020; Accepted 1 February 2020

Available online 4 February 2020

2211-2855/© 2020 Elsevier Ltd. All rights reserved.

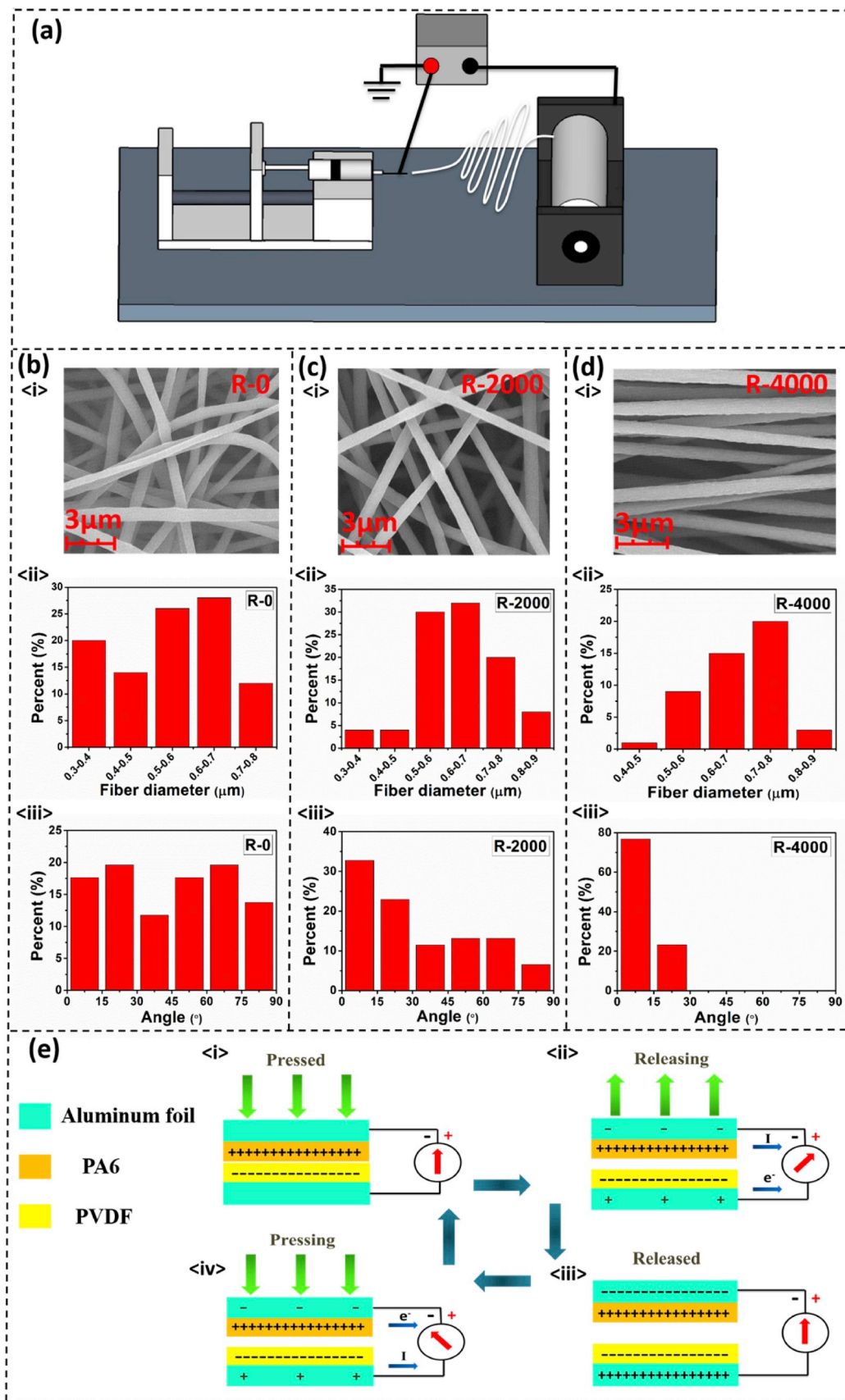


Fig. 1. (a) Schematic diagram of the electrospinning device. (i) SEM image, (ii) diameter distribution and (iii) orientation degree distribution of the electrospun PVDF nanofibers in the case of (b) R-0, (c) R-2000, (d) R-4000. (e) The working principle of the TENG in contact-separation mode.

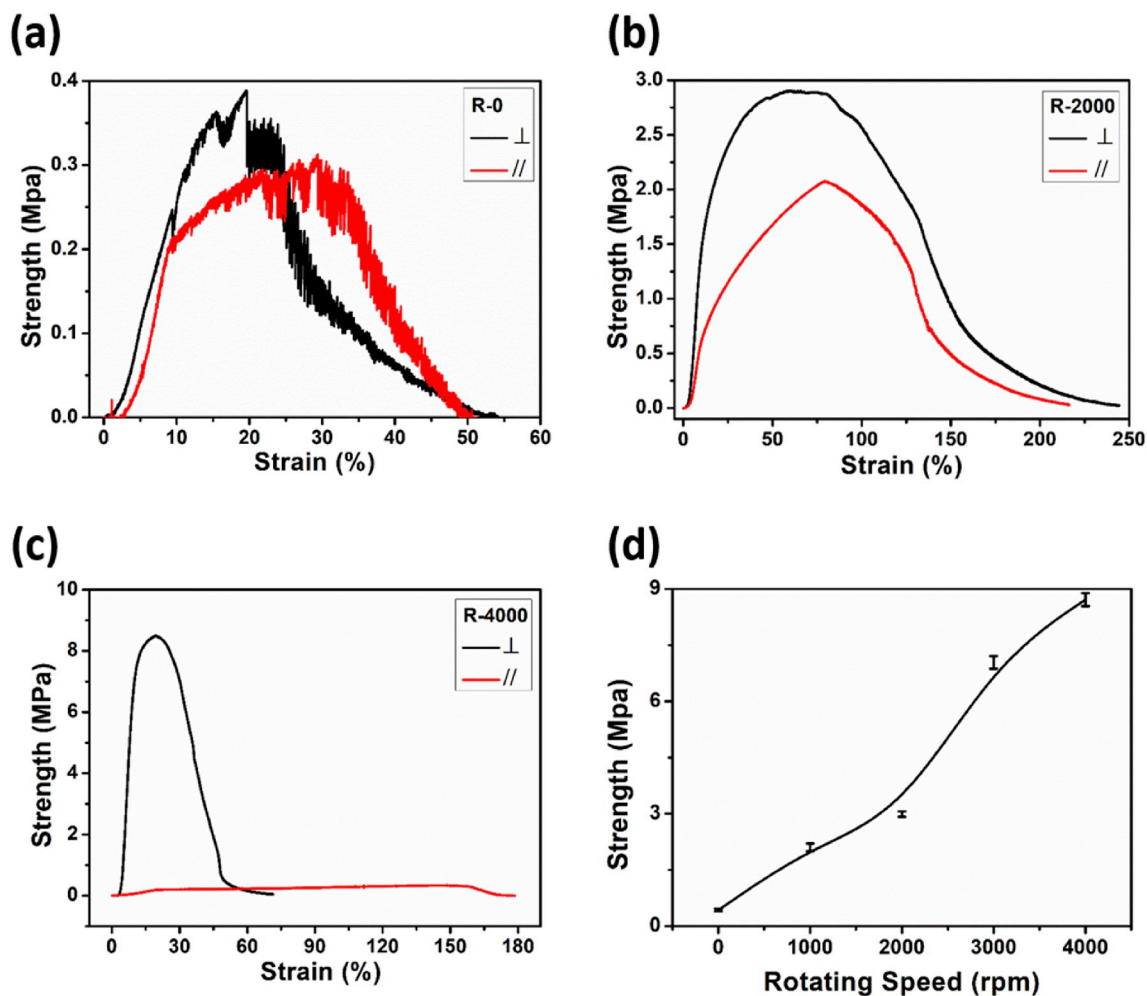


Fig. 2. Tensile properties of electrospun PVDF fibers at (a) R-0, (b) R-2000, (c) R-4000. (d) When the PVDF fiber membrane is stretched in the \perp direction, the tensile properties of the PVDF fibers are related to the rotating speed of the roller.

the same, and the anisotropic output can easily determine the fiber arrangement direction, A-TENG can be a good anticounterfeiting method.

2. Experimental section

2.1. Materials

Polyvinylidene fluoride (PVDF) powders ($M_w \sim 1000000$, Shanghai 3F New Materials Co., Ltd.), and Nylon 6 (PA6) powders (Macklin Biochemical Co., Ltd., China) were used in this study. N, N-dimethylformamide (DMF), formic acid, acetic acid and ethanol were obtained from Sinopharm Chemical Reagent Co., Ltd. Acetone was obtained from Laiyang Fine Chemical Factory, China.

2.2. Preparation of solutions for electrospinning

The PVDF powder was dissolved in acetone-DMF solvent mixture (1/1 w/w) to obtain PVDF homogeneous solution with a concentration of 10 wt%. Afterwards, the mixture was stirred at 40°C for 4 h with a magnetic stir bar to prepare a PVDF solution. A PA6 homogeneous solution having a concentration of 15 wt% was prepared, and the PA6 powder was dissolved in a formic acid-acetic acid solvent mixture (1/1 w/w), followed by stirring at room temperature for 4 h.

2.3. Fabrication of the NG

Fig. 1a shows a schematic of the electrospinning process. The aluminum foil was fixed on a roller collector with a radius of 37.4 mm, the PVDF nanofiber membrane was prepared by electrospinning as the TENG negative material, and the PA6 nanofiber membrane was used as the TENG positive material [38]. The PVDF nanofiber membrane was prepared at a temperature of $23 \pm 3^\circ\text{C}$ and a humidity of $40 \pm 5\%$. The needles used had an inner diameter of 0.6 mm and an outer diameter of 0.91 mm. Electrospinning solution is 5 mL. The polymer solution was loaded at a constant flow rate of 1 mL h^{-1} , a high voltage of 15 kV was applied, the distance between the roller collector and the spinneret was 15 cm, and the roller's rotating speed was adjusted to collect PVDF nanofibers of different order.

2.4. Characterization and measurements

The surface morphology and microstructure of TENG were measured by scanning electron microscopy (SEM, TM-1000, Hitachi). The crystal structure of the PVDF powder and fibers were analyzed by receiving an X-ray diffraction (XRD) pattern on a diffractometer (Rigaku, SmartLab). The infrared absorption spectrum of the PVDF fiber membrane and PA6 fiber membrane were obtained by Fourier transform infrared spectroscopy (FTIR, Thermo Scientific Nicolet iN10). The output current signals of TENG were recorded by a picoammeter (Keithley 6487), a current amplifier (SR570) and a digital oscilloscope (GDS-2102, Gwinstek). The

output voltage signals were recorded by a digital oscilloscope (GDS-2102, Gwinstek). The charging voltages of the capacitor were measured by a digital multimeter (Rigol DM 3058). The stress strain of the PVDF fiber membrane was measured by Instron 3300 Universal Testing Systems. The compression properties of the PVDF fiber membrane were recorded by a digital display force gauge ZP-500. Ultra-high speed information acquisition card (USB-HRF4826) was used to collect multi-channel output signals. In order to generate triboelectric electricity through NG, we used a self-made device that can exert periodic contact; the schematic and working principle of the device are shown in Fig. S1.

3. Results and discussion

3.1. The basic characterization of the TENG

Fig. 1a shows the electrospinning device, which is mainly composed of a roller, a propulsion pump and a power source. The long axis is defined as the direction along the rotating of the roller, and the orientation angle (θ) of the fiber is the difference in angle between the fiber and the long axis, so that the distribution of the degree of orientation (γ) can be obtained. We define γ as the percentage of fiber with an orientation angle close to θ .

Fig. 1b shows <i> the SEM image, <ii> the fiber diameter distribution and <iii> the fiber orientation distribution of the spun PVDF nanofibers when electrospinning is performed directly without using a roller (R-0), it can be seen that the distribution of nanofibers in all directions showed no obvious difference. Fig. 1c shows <i> the SEM image, <ii> the fiber diameter distribution and <iii> the fiber orientation distribution of the PVDF nanofibers spun by electrospinning when the roller's rotating speed is 2000 rpm (R-2000). For this sample, the fiber arrangement in each direction is different, and the order arrangement of the fibers is arising. Fig. 1d shows <i> the SEM image, <ii> the fiber diameter distribution and <iii> the fiber orientation distribution of the PVDF nanofibers spun by electrospinning when the rotating speed is 4000 rpm (R-4000), it can be seen that the fibers are significantly ordered. The SEM images of the electrospun PVDF nanofibers at a rotating speed of 500 rpm, 1000 rpm, and 3000 rpm are shown in Fig. S2a, S2b and S2c and we can see that higher ordering can be obtained from higher rotating speed. Fig. S2 shows (d) the SEM image, (e) the fiber diameter distribution and (f) the fiber orientation distribution of the PA6 nanofibers spun by electrospinning when the roller's rotating speed is 4000 rpm.

TENG is based on the composite principle of triboelectric charging and electrostatic induction to realize the conversion of mechanical energy to electrical energy. Fig. 1e shows the contact-separation TENG consisting of two triboelectric layers with different electronegativity and two electrodes. We chose PA6 nanofibers and PVDF nanofibers as positive and negative triboelectric layers, respectively. In the original state (state i), the PVDF fiber membrane was in contact with the PA6 fiber membrane, and no potential difference was generated. Due to the different electronegativity, the charge will be transferred from the surface of the PA6 fiber membrane to the surface of the PVDF fiber membrane. Net positive charges are left on the surface of the PA6 nanofiber, while net negative charges are left on the surface of the PVDF nanofiber, keeping electrostatic equilibrium. When the two fiber membranes are separated, the relative motion between the opposite charges destroys the existing electrostatic equilibrium, which establishes a potential difference between the electrodes and drives the free electron flow between the electrodes to rebalance the electrostatic field, causing current flow (state ii). When the maximum separation distance is reached, the current vanishes (state iii). When the two charged triboelectric layers are in contact again, the current is reversed (state iv) [30,39–42].

As shown in Fig. 2, the direction parallel to the surface of the drum is defined as a transverse direction (\parallel), and a direction perpendicular to the surface of the drum, that is, a direction in which the drum rotates is defined as a longitudinal direction (\perp).

The tensile properties of the PVDF fiber membrane fabricated under various rotating speed were respectively tested in the \parallel direction and the \perp direction. The ambient humidity is $42 \pm 2\%$, the temperature is $26 \pm 2^\circ\text{C}$, the tensile rate is 2 mm/min, the test sample size is 2 cm*1 cm, and 4 samples are tested for each rotation speed. The tensile strength is obtained by

$$P = F / (h * d) \quad (1)$$

where h is the thickness of the film, d is the sample width. The thickness of the test sample is shown in Fig. S3. As shown in Fig. 2a, for R-0, the PVDF spun fibers are arranged in disorder, take two directions perpendicular to each other, and mark them as \parallel direction and the \perp direction, the difference in tensile properties between the \parallel direction and the \perp direction is not large, and the tensile strength is about 0.3 MPa. As the rotating speed of the roller increases, the order degree of the fiber increases, and the tensile strength of the fiber film stretched in the \perp direction becomes higher and higher. For R-4000, the \perp tensile strength reaches 8.5 MPa, the difference of tensile strength between the \parallel and the \perp is large, and the \parallel tensile strength is only 0.33 MPa, as shown in Fig. 2c, showing significant anisotropy.

The tensile properties of the PVDF fibers at 500 rpm, 1000 rpm, and 3000 rpm were also tested, and the reference data is shown in Fig. S4. Fig. 2d shows the relationship between the tensile strength in the \perp direction and the rotating speed of the roller. It can be clearly seen that the tensile strength of the PVDF fiber increases as the rotating speed of the roller increases. This is because the non-Gaussian broadening of the stress probability density function under tensile load increases with the increase of porosity and disorder. Ordering averages the load, leading to gradual transitions from single pore stress concentration state to porous interaction [37]. Demonstration animation can be referred to the supplemental information Video S1.

Supplementary video related to this article can be found at <https://doi.org/10.1016/j.nanoen.2020.104572>.

Unlike the \perp tensile properties, since the \parallel direction doesn't rely on the rotating speed of the roller, there is no regularity in the \parallel tensile properties. This leads to an obvious anisotropic mechanical property. The rotating speed can affect the strength of the membrane along both directions. At an appropriate rotating speed, the mechanical strength along both directions is strengthened. Meanwhile, the elongations at break along both directions are greatly improved. This method may also be applicable to other fiber membranes. In the actual use process, compression will hardly damage the nanogenerator, and the fiber membrane can be compacted quickly, so it only responds elastically to small pressures. We test the compression performance, the fiber membrane was fixed on a glass piece having a thickness of 0.147 mm, compressed at a rate of 110 $\mu\text{m}/\text{m}$ in using a precision propulsion device, and the compression area was 9.62 mm^2 . The compression properties of PVDF fiber membranes are shown in Fig. S4d, and for larger force the compress will be the elastic response of the test instrument. In order to analyze the material structure of the material, FTIR and XRD test were also performed. The FTIR of PVDF and PA6 fibers are described in Supplementary Data Figs. S5a and S5b, the XRD of PVDF are described in Figs. S5c and S5d.

3.2. The electrical performance of TENG

In order to test the performance of the manufactured anisotropic TENG (A-TENG, length, 40 mm; width, 40 mm) to collect environmental mechanical energy, the short-circuit current and open-circuit voltage of this generator were systematically studied. The PVDF friction layer is 0.068 mm and the PA6 friction layer is 0.03 mm in thickness. In order to ensure the effect of eliminating the thickness of the fiber membrane on the experimental results, the same pair of samples was used during the test. The A-TENG is placed on the reciprocating device as shown in Fig. S1 to complete the contact-separation of the A-TENG. Its various

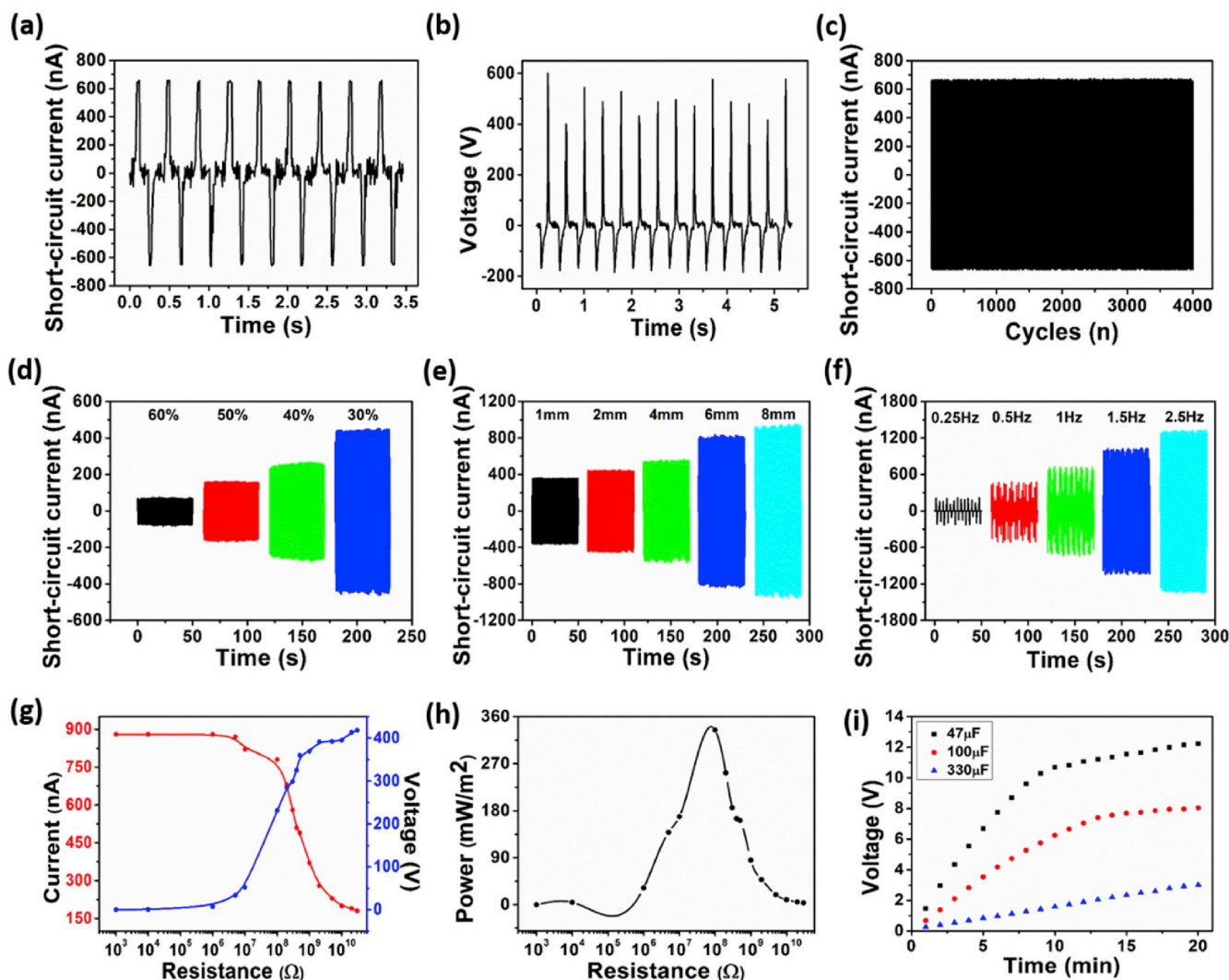


Fig. 3. Electrical performance of TENG. (a) Short-circuit current and (b) open-circuit voltage of TENG under a mechanical frequency of 2.5 Hz with respect to time. (c) TENG's electrical durability and stability performance. The short-circuit current of TENG at different (d) environment humidity, (e) gap distance between the triboelectric layers, and (f) impact frequency. (g) Dependence of TENG's output current and voltage on external load resistance. (h) Dependence of TENG's output power on load resistance. (i) TENG charging curves for 47 μF , 100 μF and 330 μF commercial capacitors.

performances are shown in Fig. 3. As shown in Fig. 3a and b, when the ambient humidity is kept 30%, the impact frequency is kept 2.5 Hz, and the gap distance between the triboelectric layers is set 4 mm, the short-circuit current is 648 nA. When the ambient humidity is 30%, the impact frequency is 2.5 Hz, and the gap distance between the triboelectric layers is 8 mm, the open circuit voltage output is measured to be 603 V.

Long-term stability/durability is an important requirement of TENG in practical applications. The ambient humidity is 30%, the impact frequency is 2.5 Hz, the gap distance between the triboelectric layers is 4 mm, and A-TENG is tested for 4000 cycles under the repeating contact-separation, and the output performance of A-TENG before and after continuous operation was compared. As shown in Fig. 3c, there is no decrease in the short-circuit current, which indicates that A-TENG has good durability.

In order to evaluate the environmental suitability of the manufactured A-TENG, comparative experiments were performed using the control variable method to test the output performance under different environmental humidity, impact frequency, and gap distance between the triboelectric layers. Ambient humidity will significantly affect the output performance of A-TENG. The storage time of the surface triboelectric charge will be reduced in high humidity environment and thus the output will be reduced [43]. As shown in Fig. 3d, the impact

frequency is 2.5 Hz, the gap distance between the triboelectric layers is 2 mm, the short-circuit current increases with the environmental humidity decrease. Similarly, the open circuit voltage also increases as the ambient humidity decrease, as shown in Fig. S6a. This indicates that the A-TENG works better in a drier environment. As shown in Fig. 3e, the ambient humidity is 30% and the impact frequency is 2.5 Hz, the short circuit current of A-TENG increases as the gap distance between the triboelectric layers increases [39,44,45]. Fig. 3f shows that the short-circuit current increases with the increase of the impact frequency. The ambient humidity is 20% and the gap distance between the triboelectric layers is 8 mm. A higher impact frequency can reduce the duration of the current peak, thereby increasing the magnitude of the short circuit current. Accordingly, the open circuit voltage also increases as the impact frequency and the gap distance between the triboelectric layers increase, as shown in Figs. S6b and S6c.

The change of the electrical output with the load resistance was systematically studied. As shown in Fig. 3g, it can be seen that the voltage increases as the load resistance increases, while the current tends to be opposite. We obtained the power curve by Equation $P = \frac{U^2}{R}$, as shown in Fig. 3h. The maximum load power density is 0.34 W m^{-2} , when the external load resistance is 78.53 M Ω . The corresponding load voltage is 213.45 V and the current is 768.07 nA.

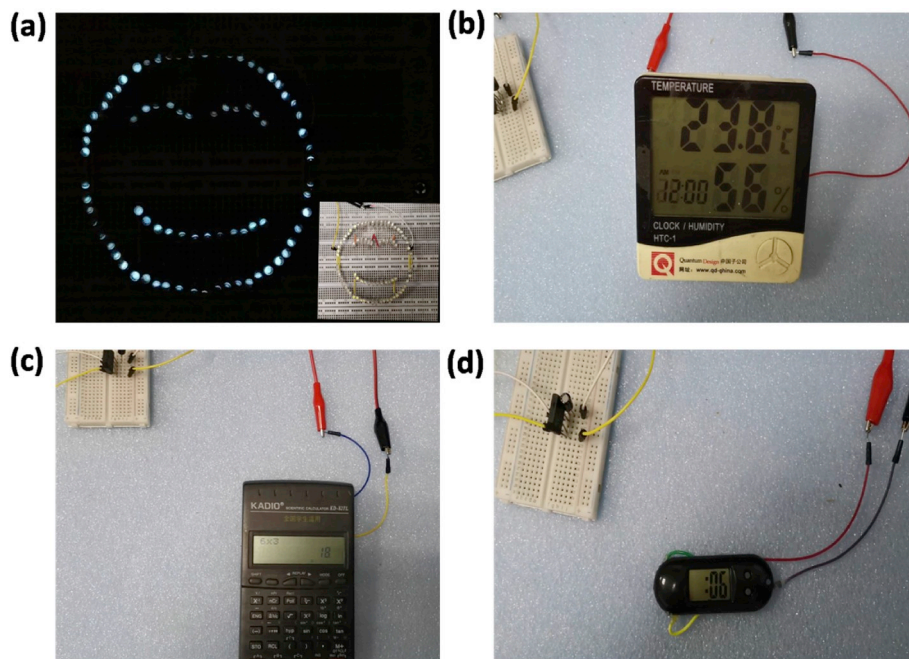


Fig. 4. Application of a circular A-TENG with $R = 4$ cm to power multiple devices. (a) Store the energy collected by A-TENG in a $100 \mu\text{F}$ commercial capacitor to illuminate the LED in the shape of a smile. Use A-TENG to drive electronic devices such as (b) temperature-humidity sensor, (c) calculator and (d) electronic watch.

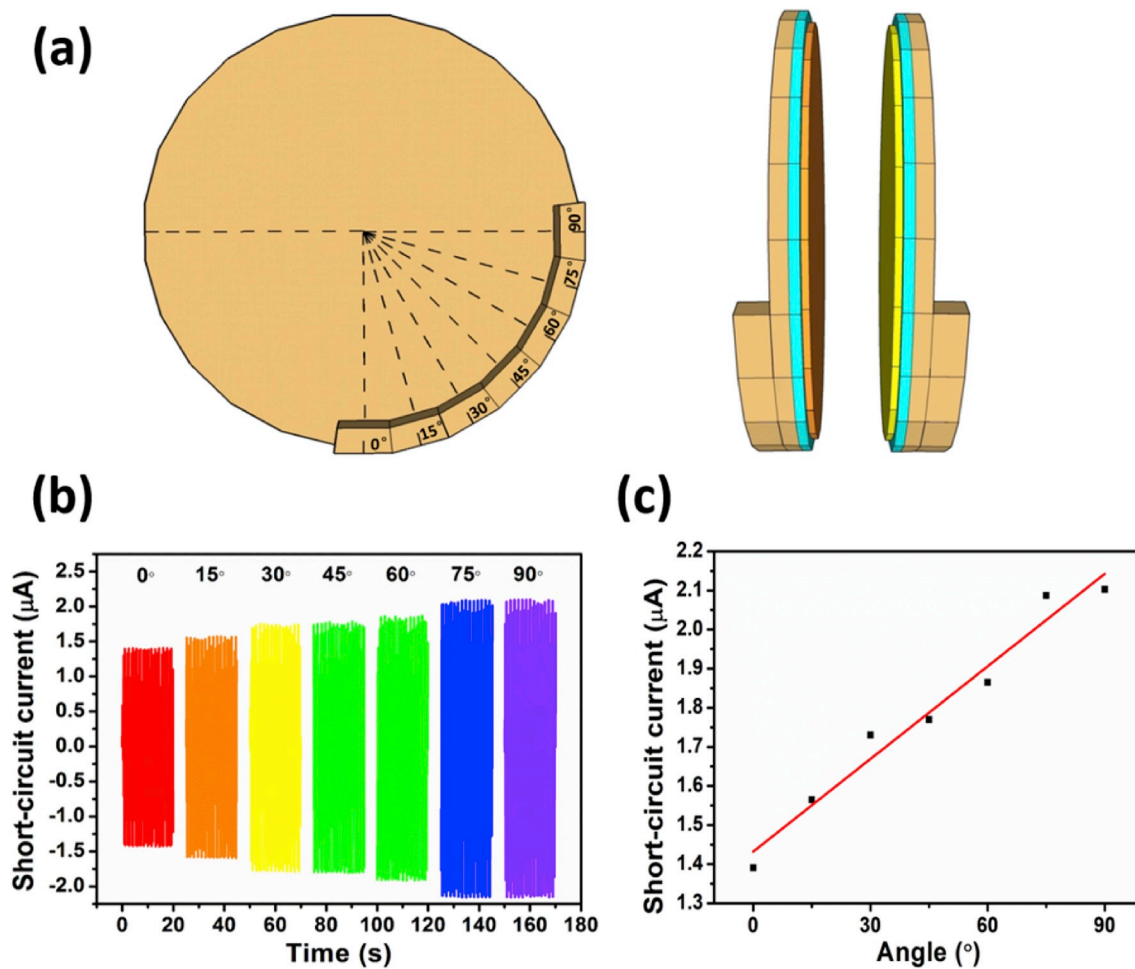


Fig. 5. (a) A-TENG angle sensor diagram. (b) The short-circuit current output signal and (c) its fitting curve when nanogenerator friction layer is rubbed at different angles.

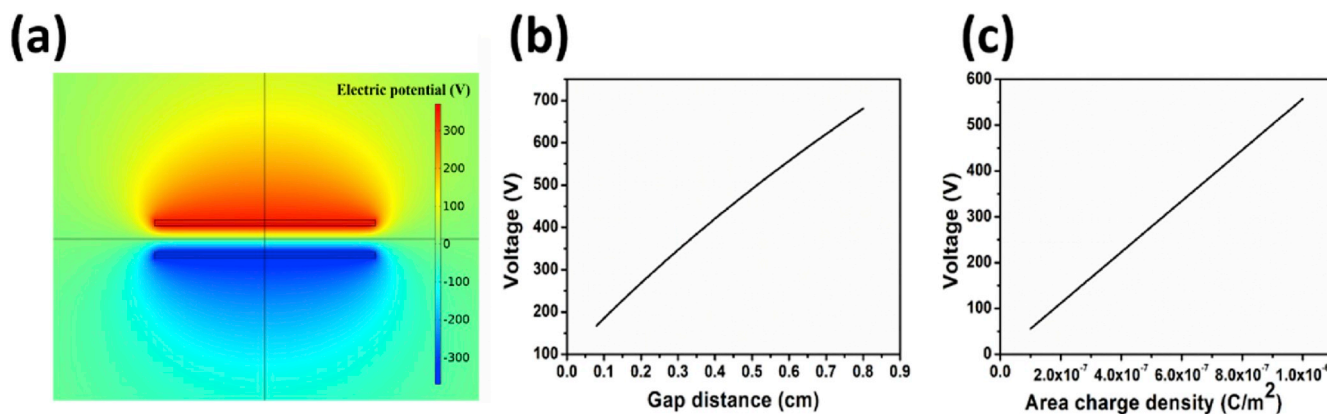


Fig. 6. (a) Electric field distribution at 0.7 cm gap after PA6-PVDF frictional charging. (b) The relationship of the potential difference between the two electrodes and the gap distance. (c) Changes in electrode potential differences caused by changes in area charge density.

In addition, output energy from A-TENG can be stored to provide continuous output. As shown in Fig. 3i, different commercial capacitors were charged in the same environment using A-TENG. For example, a 47 μF commercial capacitor can be charged up to 12.24 V at an operating frequency of 2.5 Hz. The stored energy can power small portable intelligent electronic devices. By properly designing the self-powered system, it is possible to get rid of batteries that are harmful to the environment. Meanwhile, the flexibility of the electronic system can also be increased.

As a good energy source, A-TENG can power a variety of different forms of electronic equipment. Visual demonstrations were made with a circular A-TENG with a radius of 4 cm. As shown in Fig. 4a and the Video S2 in the supplementary information, A-TENG can directly illuminate the smiley-shaped LED (a total of 80 LED). In addition, A-TENG can drive a variety of small electronic devices for normal operation by charging a commercial capacitor of 100 μF to 6 V, such as temperature-humidity sensors, calculators and electronic watches. As shown in Fig. 4b–d, the demonstration operations can be referred to the supplemental information Video S3, S4 and S5. It can be seen that A-TENG has good energy harvesting capability and has great development potential in the field of portable wearable devices, which is beneficial to popularize A-TENG.

Supplementary video related to this article can be found at <https://doi.org/10.1016/j.nanoen.2020.104572>.

3.3. The application of A-TENG

In addition to powering conventional electronics, A-TENG can also be used as self-powered sensor. As shown in Fig. 5a, considering that A-

TENG has anisotropy, an angle sensor was made by a circular ($R = 4$ cm) A-TENG, and the gap distance of the friction layer is 0.7 cm. At a given frequency and gap distance, the A-TENG rubs at different friction angles to obtain different output signals. If we measure the peak current/voltage of a single waveform, different result will be given in corresponding with different friction angles, thereby achieving angle sensing, as shown in Fig. 5b. For traditional TENG (R-0), when the relative direction of the friction layer changes, the change of the output signal will not be displayed, as shown in Fig. S7. Anisotropy is the property of being directionally dependent, which implies different properties in different directions, as opposed to isotropy. It can be defined as a difference, when measured along different axes, in a material's physical or mechanical properties. So we can define the A-TENG as nanogenerators that output differently with different relative angles of the two friction layers.

The short circuit current of TENG can be described by

$$I_{sc} = \frac{dQ_{sc}}{dt} = \frac{S\sigma d_0 v(t)}{(d_0 + x(t))^2} \quad (2)$$

where the Q_{sc} the short-circuit charge, I_{sc} the short circuit current, $x(t)$ the gap between the two friction layers, S the area of the metal electrode, d_0 the effective dielectric thickness. During the test, the contact area, gap distance, dielectric layer thickness and pressure were kept constant, so the variation of short circuit current can only be affected by the effective surface charge density. And in case of A-TENG, σ is the average value of the charge on the contact surface. Considering that the pressure is the same, the charge density on the micro friction area is kept constant, so the decrease in the average surface charge density can only be due to the decrease in the effective contact area of the friction fibers.

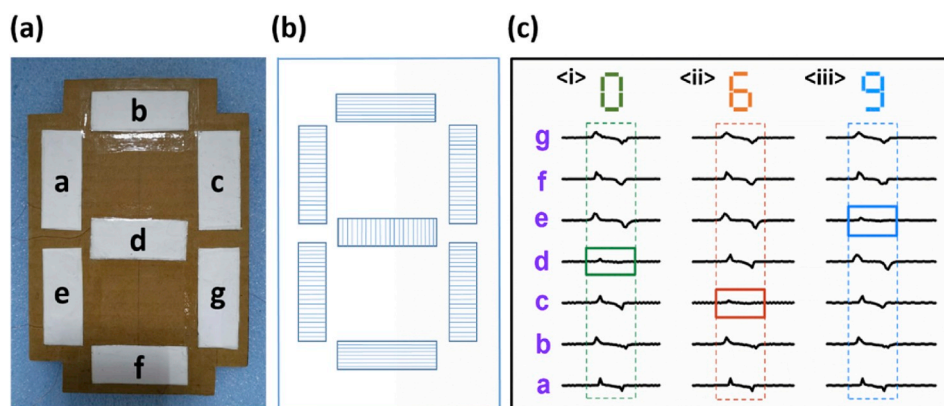


Fig. 7. (a) The number “8” is formed from PVDF ordered fiber membranes. (b) The ideal distribution of PVDF ordered fibers in the number “8”. (c) Multi-channel synchronous output signal obtained by rubbing the PA6 ordered fiber membrane with the number “8”.

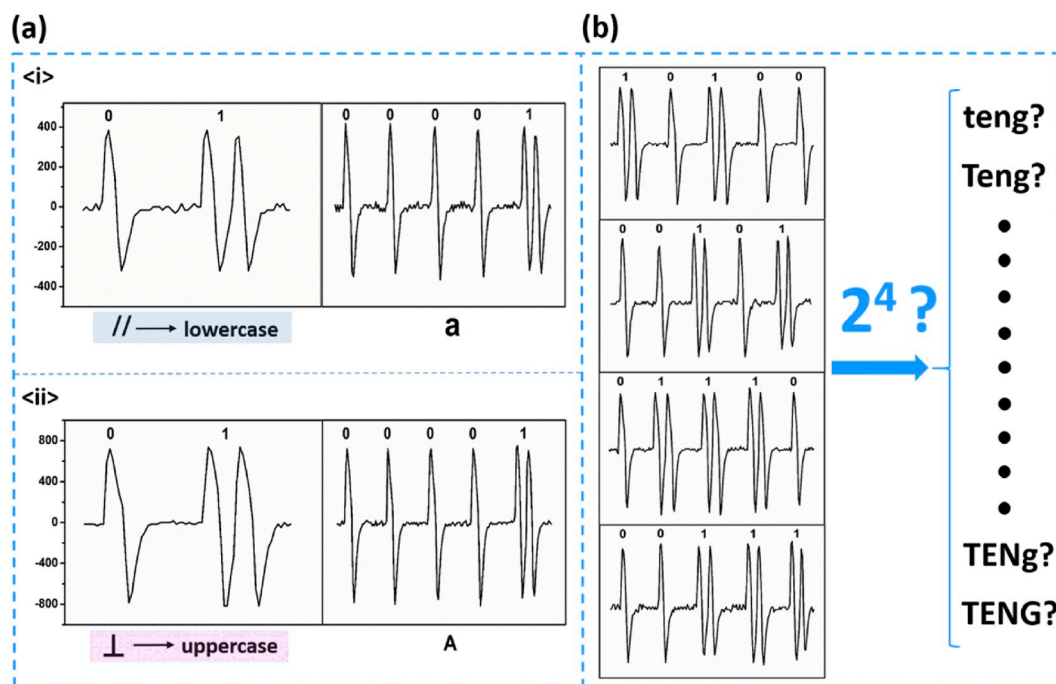


Fig. 8. (a) The single-pulse signal and the double-pulse signal are marked as “0” and “1”, respectively, with the coded letters “a” and “A” when the <i> friction layer is in parallel friction and <ii> vertical friction. (b) Use “0” and “1” to encode a group of letters. There are 2^4 combinations of case sensitivity.

Since there are gaps between adjacent fibers, when two different fiber membranes are parallel to each other (two fiber membranes are placed in the same direction), the effective contact area of the fibers is the smallest, and the output current signal is the smallest. As the contact angle increases, the effective contact area increases, and the output current signal also increases. The peak output has positive correlation with angle, so the angle can be characterized by peak current or voltage. It can be seen from Fig. 5c that the measurement angle is linear with the maximum current. The signal of the self-powered sensor did not change significantly before and after the introducing additional resistance, which is a common source of interference when using sensors in a flexible environment. Therefore, such self-powered sensor will be more reliable than the resistive sensors [30].

This analysis can be further confirmed by finite element analysis. As shown in Fig. 6, we used COMSOL to simulate a PVDF-PA6 friction nanogenerator with a radius of 4 cm. It can be seen that the positive and negative charges generated by friction respectively induce potentials of corresponding polarities on adjacent electrodes. The potential difference between the positive and negative electrodes is several hundred volts, which is in accordance with our test results. In addition, by adjusting the set gap distance, the output voltage rises approximately linearly. If the triboelectricity produces different surface charge densities, the induced potential and the surface charge density are strict linear positive correlation. It is worth mentioning that in this simulation we used a macro average charge density. In our tests, the geometry-related parameters have remained the same, so only the average charge density has changed. Considering that PA6 and PVDF have not changed during the friction process, we judge that the effective contact area at the micro level has changed, consisting with empirical judgment.

The anisotropic nanogenerator has different outputs when the relative angles of the two friction layers are different, while its appearance has no difference in these two cases, so it can be used for anticounterfeiting. Fig. 7a shows a design pattern that uses the PVDF ordered fiber membrane to spell the number “8”, which is an error message. The actual ideal fiber arrangement state is shown in Fig. 7b. Seven areas are labeled a-g, as shown in Fig. 7a. The fiber arrangement direction of the “d” position is different from that of other positions. The fibers in the

other positions are arranged horizontally, and only the fibers in the “d” position are arranged longitudinally. Using PA6 ordered fiber membrane to rubbed the sections along unique direction. The arrangement direction of the PA6 fibers is the same as the arrangement direction of the PVDF fibers at the “d” position, that is, the friction angle is 0° , and the friction angles at other positions are 90° . Waveforms of different sections were recorded by using a high-speed multifunctional synchronous data acquisition and recording system. As shown in Fig. 7c.i, the output signal at “d” is significantly smaller than the output signal at other positions. In fact, the actual output number is “0”, which can prevent forgery by others. Similarly, by changing the fiber arrangement position, other digital signals can be output, as shown in Fig. 7c.ii and iii. When the output signal at “c” is smaller than the output signal at other positions, the real number displayed is “6”. When the output signal at “e” is smaller than the output signals at other positions, the real number displayed is “9”.

A-TENG can also encrypt Morse codes to ensure communication security. The single-pulse signal and double-pulse signal of A-TENG represent “0” and “1”, respectively, and the 26 letters are encoded by “0” and “1”. The details are encoded in the [Supplementary Information Fig. S8](#). As shown in Fig. 8a, the two friction layer fibers are placed in parallel (||), that is, when the friction angle is 0° and placed vertically (\perp), that is, when the friction angle is 90° , the peak height of the pulse is significantly different, so the codes can be distinguished information. When two friction layer fibers are placed parallel, the letter is coded in lowercase, for example, “a” is coded with “00001”. When two friction layer fibers are placed perpendicular, the letter is coded in uppercase, for example, “A” is coded with the same “00001”. A group of letters are encoded with the numbers “0” and “1”, as shown in Fig. 8b. It is easy to discern what the coded letter information is through decoding waveform, but it is difficult to distinguish whether the represented letters are uppercase or lowercase. There are 2^4 possibilities, which greatly increases the difficulty of forgery. The true information can only be transmitted by testing the peak height of the pulse. The information can be encrypted well through a suitable set of precoding equipment, and the real message can only be recovered by comparing the state of the corresponding channel by the pre-given key.

4. Conclusion

In summary, we have successfully prepared aligned polymer nanofibers using high-speed roller as collector and A-TENG was prepared. Stress-strain tests have shown that both the strength and the stretchability of A-TENG are greatly improved, which can be attributed to the dispersion of stress by ordered fibers. The A-TENG can output current of 648 nA and open circuit voltage of 603 V with a maximum output power density of 0.34 W m^{-2} . The A-TENG can directly illuminate 80 LEDs. By charging a $100 \mu\text{F}$ capacitor, this nanogenerator powers the temperature-humidity sensor, calculator and electronic watch. Using the anisotropy of the material itself, this A-TENG can be used as a self-powered angle sensor. A-TENG can be a good anticounterfeiting method by using the features that the membrane looks the same and outputs differently along different directions. In addition, A-TENG's application in information encryption has also been developed.

Declaration of competing interest

The authors declare that they have no known competing financial interests or personal relationships that could have appeared to influence the work reported in this paper.

Acknowledgements

This work was supported by the National Natural Science Foundation of China (51673103, 51973100 and 11847135).

Appendix A. Supplementary data

Supplementary data to this article can be found online at <https://doi.org/10.1016/j.nanoen.2020.104572>.

References

- J. Chen, Y. Huang, N. Zhang, H. Zou, R. Liu, C. Tao, X. Fan, Z.L. Wang, *Nat. Energy* 1 (2016) 16138.
- Z.L. Wang, J. Chen, L. Lin, *Energy Environ. Sci.* 8 (2015) 2250–2282.
- Z.L. Wang, *Mater. Today* 20 (2017) 74–82.
- Z. Lin, B. Zhang, H. Zou, Z. Wu, H. Guo, Y. Zhang, J. Yang, Z.L. Wang, *Nano Energy* 68 (2020) 104378.
- Z. Quan, C.B. Han, T. Jiang, Z.L. Wang, *Adv. Energy Mater.* 6 (2016) 1501799.
- R. Pan, W. Xuan, J. Chen, S. Dong, H. Jin, X. Wang, H. Li, J. Luo, *Nano Energy* 45 (2018) 193–202.
- K. Dai, X. Wang, F. Yi, C. Jiang, R. Li, Z. You, *Nano Energy* 45 (2018) 84–93.
- W. Xu, L.B. Huang, M.C. Wong, L. Chen, G. Bai, J. Hao, *Adv. Energy Mater.* 7 (2017) 1601529.
- J. Sun, X. Pu, M. Liu, A. Yu, C. Du, J. Zhai, W. Hu, Z.L. Wang, *ACS Nano* 12 (2018) 6147–6155.
- J. Deng, X. Kuang, R. Liu, W. Ding, A.C. Wang, Y.C. Lai, K. Dong, Z. Wen, Y. Wang, L. Wang, *Adv. Mater.* 30 (2018) 1705918.
- F.-R. Fan, L. Lin, G. Zhu, W. Wu, R. Zhang, Z.L. Wang, *Nano Lett.* 12 (2012) 3109–3114.
- S.K. Karan, R. Bera, S. Paria, A.K. Das, S. Maiti, A. Maitra, B.B. Khatua, *Adv. Energy Mater.* 6 (2016) 1601016.
- S. Siddiqui, H.B. Lee, D.I. Kim, L.T. Duy, A. Hanif, N.E. Lee, *Adv. Energy Mater.* 8 (2018) 1701520.
- W. Wu, *Nanotechnology* 27 (2016) 112503.
- S.-H. Baek, I.-K. Park, *Nanotechnology* 28 (2017), 095401.
- X. Wang, W.-Z. Song, M.-H. You, J. Zhang, M. Yu, Z. Fan, S. Ramakrishna, Y.-Z. Long, *ACS Nano* 12 (2018) 8588–8596.
- Z.L. Wang, J. Song, *Science* 312 (2006) 242–246.
- J. Kwon, W. Seung, B.K. Sharma, S.-W. Kim, J.-H. Ahn, *Energy Environ. Sci.* 5 (2012) 8970–8975.
- W. Guo, C. Tan, K. Shi, J. Li, X.-X. Wang, B. Sun, X. Huang, Y.-Z. Long, P. Jiang, *Nanoscale* 10 (2018) 17751–17760.
- Y. Yang, Y. Zhou, J.M. Wu, Z.L. Wang, *ACS Nano* 6 (2012) 8456–8461.
- X. Wang, Y. Dai, R. Liu, X. He, S. Li, Z.L. Wang, *ACS Nano* 11 (2017) 8339–8345.
- F. Gao, W. Li, X. Wang, X. Fang, M. Ma, *Nano Energy* 22 (2016) 19–26.
- J. Qi, N. Ma, Y. Yang, *Adv. Mater. Interface* 5 (2018) 1701189.
- M.-H. You, X.-X. Wang, X. Yan, J. Zhang, W.-Z. Song, M. Yu, Z.-Y. Fan, S. Ramakrishna, Y.-Z. Long, *J. Mater. Chem. A* 6 (2018) 3500–3509.
- Y. Yang, W. Guo, K.C. Pradel, G. Zhu, Y. Zhou, Y. Zhang, Y. Hu, L. Lin, Z.L. Wang, *Nano Lett.* 12 (2012) 2833–2838.
- R. Que, M. Shao, S. Wang, D.D.D. Ma, S.-T. Lee, *Nano Lett.* 11 (2011) 4870–4873.
- W.Z. Song, X.X. Wang, H.J. Qiu, Q. Liu, J. Zhang, Z.Y. Fan, M. Yu, S. Ramakrishna, H. Hu, Y.Z. Long, *Nano Energy* 63 (2019) 103878.
- F.R. Fan, W. Tang, Z.L. Wang, *Adv. Mater.* 28 (2016) 4283–4305.
- X.-S. Zhang, M.-D. Han, R.-X. Wang, B. Meng, F.-Y. Zhu, X.-M. Sun, W. Hu, W. Wang, Z.-H. Li, H.-X. Zhang, *Nano Energy* 4 (2014) 123–131.
- H.-J. Qiu, W.-Z. Song, X.-X. Wang, J. Zhang, Z. Fan, M. Yu, S. Ramakrishna, Y.-Z. Long, *Nano Energy* 58 (2019) 536–542.
- X. Chen, S. Xu, N. Yao, Y. Shi, *Nano Lett.* 10 (2010) 2133–2137.
- L. Gu, N. Cui, L. Cheng, Q. Xu, S. Bai, M. Yuan, W. Wu, J. Liu, Y. Zhao, F. Ma, *Nano Lett.* 13 (2012) 91–94.
- W. Du, J. Nie, Z. Ren, T. Jiang, L. Xu, S. Dong, L. Zheng, X. Chen, H. Li, *Nano Energy* 51 (2018) 260–269.
- J. Song, L. Gao, X. Tao, L. Li, *Mater* 11 (2018) 2120.
- D. Sun, C. Chang, S. Li, L. Lin, *Nano Lett.* 6 (2006) 839–842.
- G.S. Bisht, G. Canton, A. Mirsepassi, L. Kulinsky, S. Oh, D. Dunn-Rankin, M. J. Madou, *Nano Lett.* 11 (2011) 1831–1837.
- H. Laubie, F. Radjai, R. Pellenq, F.-J. Ulm, *Phys. Rev. Lett.* 119 (2017), 075501.
- H. Zou, Y. Zhang, L. Guo, P. Wang, X. He, G. Dai, H. Zheng, C. Chen, A.C. Wang, C. Xu, *Nat. Commun.* 10 (2019) 1427.
- Z. Li, J. Shen, I. Abdalla, J. Yu, B. Ding, *Nano Energy* 36 (2017) 341–348.
- B.D. Chen, W. Tang, C. He, C.R. Deng, L.J. Yang, L.P. Zhu, J. Chen, J.J. Shao, L. Liu, Z.L. Wang, *Mater. Today* 21 (2018) 88–97.
- M. Willatzen, Z.L. Wang, *Nano Energy* 52 (2018) 517–523.
- Z.L. Wang, *ACS Nano* 7 (2013) 9533–9557.
- V. Nguyen, R. Zhu, R. Yang, *Nano Energy* 14 (2015) 49–61.
- S. Niu, Z.L. Wang, *Nano Energy* 14 (2015) 161–192.
- S. Niu, S. Wang, L. Lin, Y. Liu, Y.S. Zhou, Y. Hu, Z.L. Wang, *Energy Environ. Sci.* 6 (2013) 3576–3583.



Xiao-Xiong Wang received the Ph.D. degree in University of Science and Technology of China in 2016. His research fields cover electrospinning of magnetic materials, electrospun nanogenerators and their applications, infrared radiative cooling materials.



Ning Wang received her BS degree from Ludong University in 2017. Now she is studying for her master's degree at Qingdao University (with Prof. Yun-Ze Long). Her current research interests are focused on electrospinning techniques, nanogenerator and their applications.



Hui-Jing Qiu received her BS degree from University of Jinan in 2017. Now she is studying for her master's degree at Qingdao University (with Prof. Yun-Ze Long). Her current research interests are focused on triboelectric nanogenerator and self-powered electronics.



Wei-Zhi Song received his BS degree from Qingdao University in 2017. Now he is studying for his doctor's degree at Qingdao University (with Prof. Yun-Ze Long). His current research interests are focused on electrospinning techniques, nanogenerator and their applications.



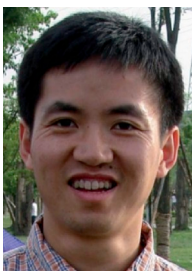
Miao Yu graduated from Nanjing University with a BS degree. He got the master's degree from Hong Kong University of Science and Technology. He has a doctoral degree from Columbia University. In 2016, he was selected as a leader in Taishan industry in Shandong Province (Taishan scholars from overseas experts in Shandong Province). His research interests focus on electrospinning and nanomaterials.



Qi Liu received his B.S. degree in Qingdao University in 2017. He started M.S. studies in Qingdao University from the fall of 2017. His research interests are mainly about electrospinning and device applications of nanofiber.



Seeram Ramakrishna received the Ph.D. from the University of Cambridge, UK in 1992. He is the Director of Center for Nanofibers and Nanotechnology at the National University of Singapore. He is an elected Fellow of UK Royal Academy of Engineering, Singapore Academy of Engineering, Indian National Academy of Engineering and ASEAN (Association of Southeast Asian Nations) Academy of Engineering & Technology. His research areas cover nanomaterials for healthcare, energy, water, and the environment.



Zhi-Yong Fan received his BSc and MSc degree from Fudan University, China, in 1998 and 2001, respectively. He received a PhD degree from the University of California, Irvine in 2006. From 2007 to 2010, he worked in the University of California, Berkeley as a postdoctoral fellow, with a joint appointment with the Lawrence Berkeley National Laboratory. In May 2010, he joined the HKUST as an Assistant Professor. His research effort concentrates on engineering novel nanostructures with functional materials, for technological applications including energy conversion, electronics and sensors.



Yun-Ze Long received his BSc degree from the University of Science & Technology of China in 2000 and received a PhD degree from the Institute of Physics, Chinese Academy of Sciences in 2005. He then worked in the Institut des Materiaux Jean Rouxel, CNRS, France, as a postdoctoral fellow. He has been with the Qingdao University since Dec. 2006, where he is currently a full Professor. From 2009 to 2011, he worked as a visiting researcher in the University of Sydney and the HKUST. His research interests focus on one dimensional functional nanomaterials.